J. Non-Newtonian Fluid Mech. 158 (2009) 6–17

Contents lists available at ScienceDirect

Journal of Non-Newtonian Fluid Mechanics

journal homepage: www.elsevier.com/locate/jnnfm

Shear rejuvenation, aging and shear banding in yield stress fluids

Andreas N. Alexandrou [a,*], Nicholas Constantinou [a], Georgios Georgiou [b]

[a] Department of Mechanical and Manufacturing Engineering, University of Cyprus, 75 Kallipoleos Str., Nicosia 20537, Cyprus
[b] Department of Mathematics and Statistics, University of Cyprus, Nicosia, Cyprus

ARTICLE INFO

Article history:
Received 1 April 2008
Received in revised form 21 January 2009
Accepted 23 January 2009

Keywords:
Herschel–Bulkley fluid
Shear banding
Shear rejuvenation
Structural parameter
Thixotropy
Yield stress

ABSTRACT

The purpose of this work is to simulate shear rejuvenation and aging effects in shear thinning yield stress fluids in a typical rotational rheometer and to provide a common framework to describe the behavior of yield stress materials in general. This is particularly important in the determination of material constants under both steady and unsteady conditions. The breakdown and buildup of structure are studied using a theory based on the Herschel–Bulkley flow model that it is consistent with experimental data. The theory is implemented using a novel computational method. Interestingly, the simulations reveal the existence of time-dependent shear banding that occurs within the gap when the macroscopically imposed shear rate is below a certain critical value. Shear banding is analyzed in detail and results showing the effects of major parameters on the phenomenon are presented.

1. Introduction

In yield stress materials a finite stress value (yield stress) must be exceeded for flow to occur; otherwise they behave as solids. A few examples are various food products (mayonnaise, ketchup), cosmetics (cold cream, make up, hair gel, shaving foam), pastes (toothpaste), emulsions, foams, polymer gels (e.g. carbopol), suspensions (oil drilling fluids like bentonite), wet and dry sand, certain clays, certain paints and printing inks, coatings, quicksand and quick clay [2–5].

The original motivation for this work [1] was our interest in the semisolid process in which specially primed metal alloys are processed in a state between that of a pure solid and a pure liquid. At rest (in the order of minutes) semisolid slurries build up structure as metal particles weld together to form a continuous solid skeleton which is responsible for the viscoplastic behavior of the slurry [1,6]. The specially prepared material is injected at very high speed into a die for the production of high integrity parts.

In most typical flowing suspensions of yield stress fluids, there coexist three types of forces [7]: (a) those of colloidal origin; (b) the Brownian (thermal) randomizing force; and (c) the viscous forces acting on the particles due to fluid flow. The interplay between these forces and their balance are responsible for the formation of an internal structure which (i) has an inherit "strength", i.e. a yield stress and (ii) it can be altered by an externally applied shear during processing. In other more specialized suspensions, the mechanisms responsible for the internal structure and the yield stress may be entirely different. In semisolid suspensions, for instance, the yield stress is the combined effect of the solid network of connected particles and the dry friction between loose particles.

Given the nature of the internal structure and its "vulnerability" to an applied shear, most suspensions exhibit not only a strong non-linear viscoplastic behavior but also a time-dependent or thixotropic behavior [9]. Fig. 1 shows typical experimental data for a semisolid suspension from a rotational experiment where the stress at the rotating surface changes with time: after a rapid decrease in the stress at the rotating cylinder with a characteristic sigmoidal variation (in a log–log representation) the stress achieves a steady-state after a long time [12]. This time-dependent behavior is due to the breakage of solid bonds formed during prolonged rest between the solid particles. It is interesting to note that for semisolid slurries the actual process is very fast with processing times in the order of 0.5 s. This coincides with the time of the fastest structural breakdown rate. This highlights the importance of considering this complex behavior in material constants for transient applications.

Other mechanisms responsible for thixotropy can be the disorganization of individual particles in granular materials, the deformation and disorganization of individual droplets changing in shape from spherical to elliptical in colloids (foams and emulsions), the orientation of polymer chains along the velocity field – as well as their breakage – in gels and the breaking of particle aggregates in suspensions. It is clear from the above that the yield stress

* Corresponding author. Tel.: +357 22892256; fax: +357 22892254.
E-mail address: andalexa@ucy.ac.cy (A.N. Alexandrou).

0377-0257/$ – see front matter © 2009 Elsevier B.V. All rights reserved.
doi:10.1016/j.jnnfm.2009.01.005

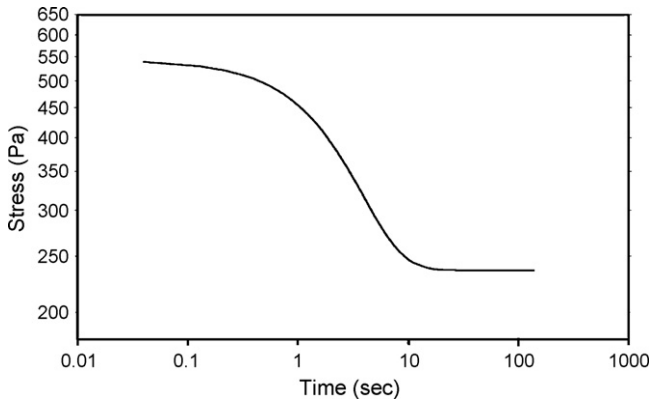

Fig. 1. A typical result for the variation of stress with time for an SSM slurry in a rotational experiment [12].

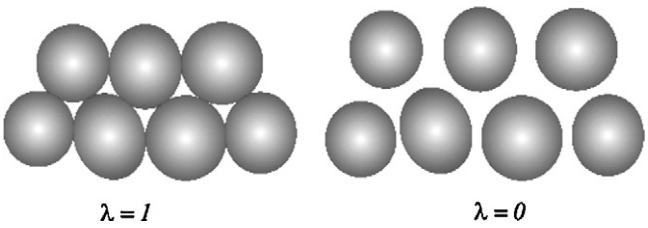

Fig. 2. Coherency parameter in a fully structured state (left) and in a fully broken state (right) [1].

and thixotropic effects are closely related and one cannot study one effect without the other.

In most suspensions there is a critical shear rate which determines the relative competition between what are known as aging and shear rejuvenation processes [14]. In shear rejuvenation as discussed above the structure breaks down resulting in decreasing viscosity with time. However, upon the reduction or the removal of shear aging occurs where the structure slowly rebuilds with a corresponding increase in the viscosity. At steady-state, the rates of shear rejuvenation and aging are equal. When shear is removed completely the viscosity eventually reaches an infinite value and the fluid finally ceases to flow [15].

Pignon et al. [16] have shown that structure buildup occurs over two distinct time scales: a short one, corresponding to relaxation of the alignment produced by the shearing after the latter is interrupted, and a long one, corresponding to a slow aggregation process which gives rise to a fractal behavior at length scales on the order of 1 mm. It is during this second stage that the continuous aggregate

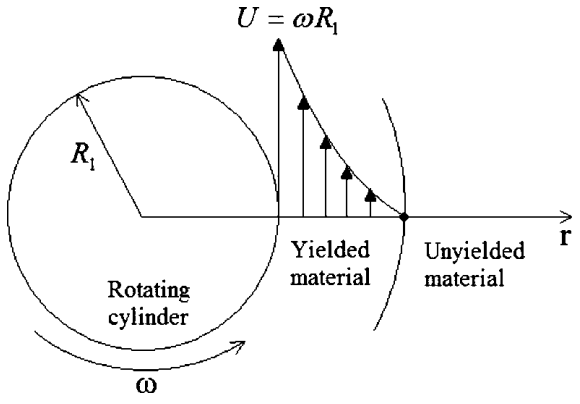

Fig. 3. Schematic of the flow geometry. The material adjacent to the rotating shaft yields, while the material away from the shaft remains unyielded [1].

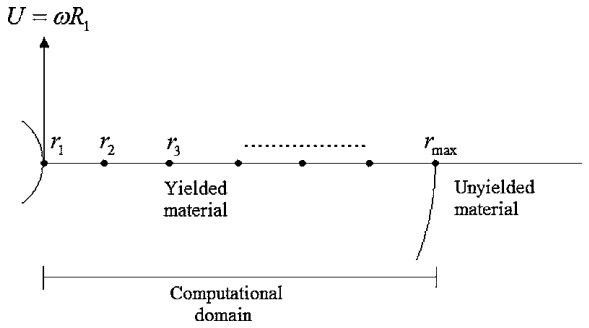

Fig. 4. The method of solution: the velocity distribution is fixed and the positions of the corresponding nodes are sought. The computational domain is in fact the yielded domain [1].

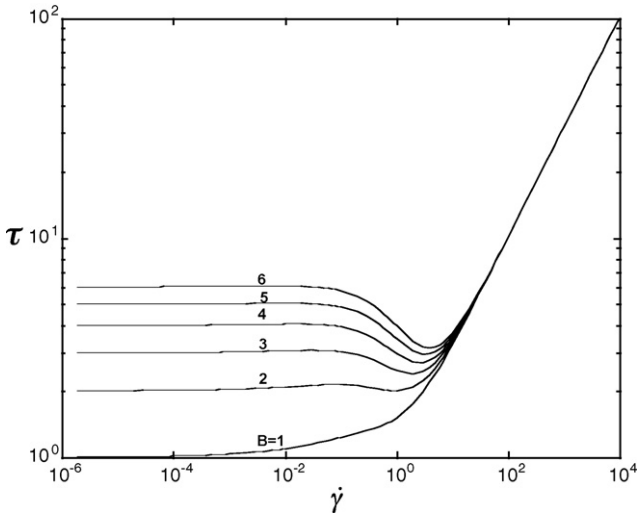

Fig. 5. Shear stress versus shear rate at equilibrium for various Bingham numbers, $\alpha_0 = \alpha_1 = \alpha_2 = 0.01$ and $n = 0.5$.

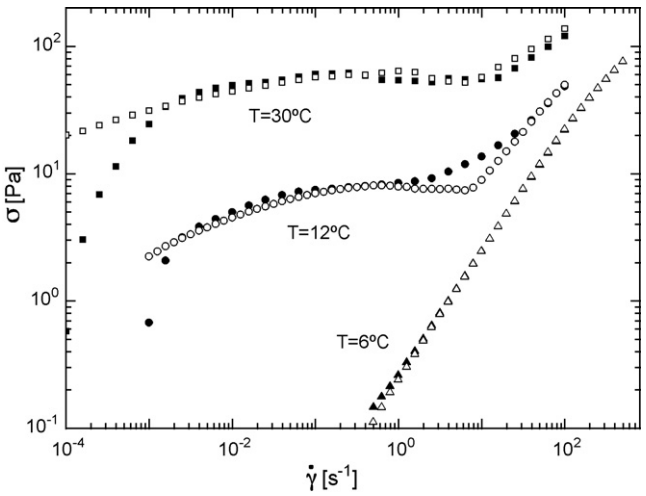

Fig. 6. Flow curves obtained from steady rate sweep measurements with the colloidal star suspension 12828 in decane (95 mg/g) at three different temperatures, 6 °C (triangles), 12 °C (circles) and 30 °C (squares). Filled symbols represent the data obtained with increasing shear from low to high; open symbols correspond to the 'return' experiment (ramp down). The measurement time per shear rate was kept constant at 14.3 s (taken from Ref. [23] with permission).

network is established, giving the suspension its yield stress fluid character [16]. The competition between aging and shear rejuvenation determines the mechanical behavior of the suspensions which is important in many applications [8,10,11,14,17].

This work focuses on both the short-term and long-term response to shear of such systems. The interest here is to study the flow details within a standard rotational rheometer which is used extensively in material characterization. Our intention is to reveal the complex phenomena that take place within the gap of the rheometer which can be critical in the evaluation of material constants.

An interesting behavior exhibited by yield stress fluids in shearing flows is that of shear banding. At sufficiently low shear rates the flow domain is divided into two parts: (a) the yielded region close to the shearing wall and (b) the unyielded or solid-like region. This is in contrast to the Herschel–Bulkley fluid model which suggests that all shear rates are possible in the material [15]. In the unyielded region no flow is observed and the shear stress must essentially be lower than the yield value of the material while in the yielded region the shear stress should be higher than the yield stress [15]. Experiments have shown that shear banding is related to a critical shear rate. Below this value the flow is localized in a region close to the shearing wall [18]. If the globally imposed shear rate increases, it is not the shear rate in the material in the yielded region that increases, but rather the extent of the sheared region which increases to fill the entire gap of the shear cell exactly at the critical shear rate [15,18–20].

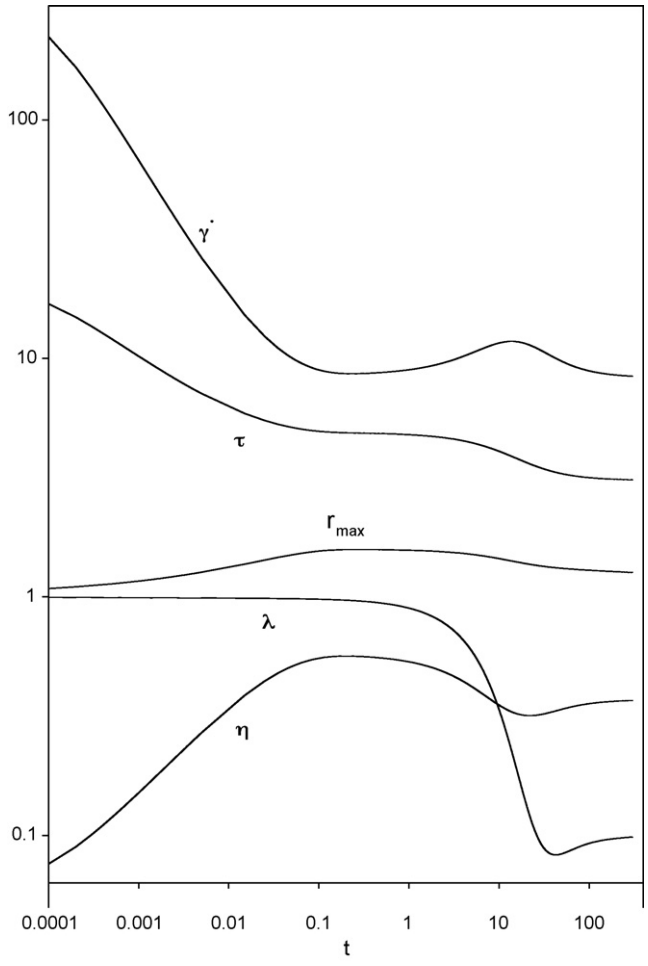

Fig. 7. Evolutions of the coherency parameter, the shear rate, the shear stress and the viscosity at the rotating surface, and of the length of the yielded domain for $B = 2$, $a_0 = a_1 = a_2 = 0.01$ and $n = 0.5$.

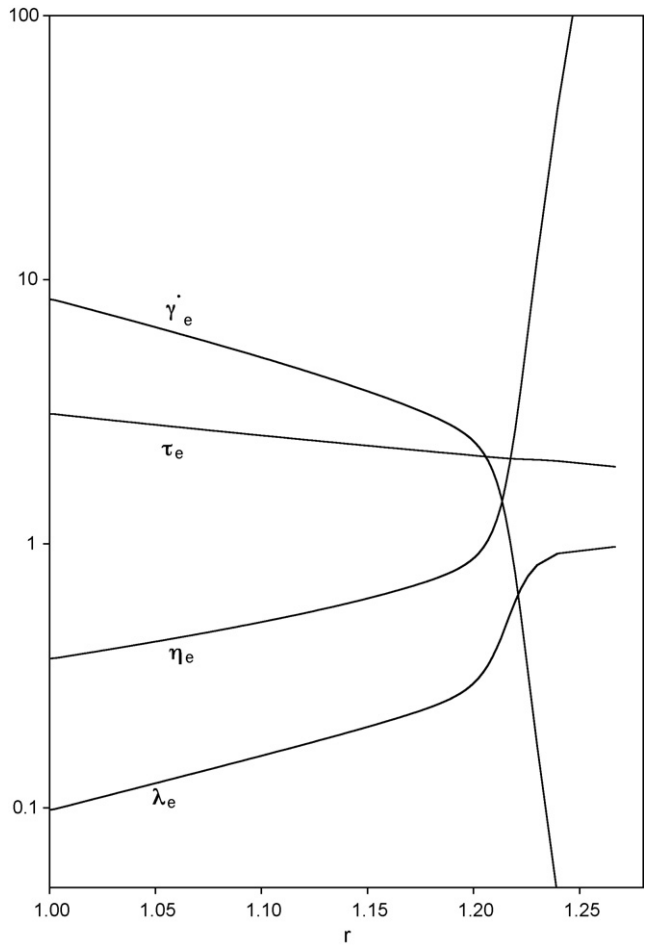

Fig. 8. Distributions of the coherency parameter, the shear rate, the shear stress and the viscosity at equilibrium for $B = 2$, $a_0 = a_1 = a_2 = 0.01$ and $n = 0.5$.

In this work, shear rejuvenation and aging effects in shear thinning yield stress fluids are simulated in a rotational rheometer. A theoretical thixotropic model, based on the H–B constitutive equation, involving a coherency parameter is proposed in Section 2. The governing equations and the method of solution of the time-dependent circular Couette flow problem are presented in Section 3. The numerical results are presented in Section 4. An interesting finding of this work is the appearance of shear banding within the gap when the imposed shear rate is below a critical value. Section 5 summarizes the conclusions.

2. Thixotropic model

To capture the evolution of the internal structure it is customarily assumed that there exists a phenomenological structural or coherency parameter λ that characterizes the state of the structure; in a fully structured state, λ is assumed to be unity, while in a fully broken state it is assumed to be zero (Fig. 2). The parameter λ can, for instance, represent the number of welded bonds in metal slurries, the organization of individual particles in granular material, the organization and form of individual droplets in colloids (foams and emulsions), the entanglement and integrity of polymer chains in gels and the integrity of particle aggregates in suspensions. The physics and evolution of λ in time are governed by appropriate evolution equations.

The rate of formation of new bonds in a suspension is typically assumed to be proportional to the concentration of particles, since

the collision probability increases with the latter. The rate of breakdown of inter-particle bonds in an average aggregate is assumed to be proportional to the number of existing bonds (structural linkages) [12]. Hence, the evolution of the structure of the suspension may be described by a kinetic equation for the coherency parameter λ of the type:

$$\frac{D\lambda}{Dt} = \alpha_0(1-\lambda) - \alpha_1\lambda\dot{\gamma}\, e^{\alpha_2\dot{\gamma}} \tag{1}$$

where $D\lambda/Dt$ is the material derivative, α_0 is the recovery parameter, α_1 and α_2 are breakdown parameters, and $\dot{\gamma}$ is the magnitude of the rate of strain. The first term in the RHS of Eq. (1) describes the aging effect and the second one accounts for the shear rejuvenation. The exponential dependence on the deformation rate is included to account for the fact that the shear stress evolution in shear rate step-up experiments is typically faster than in step-down ones [21,22].

At very low or zero shear rates, aging dominates and the structure builds-up at a constant rate of $\alpha_0(1-\lambda)$ or $1/T_0$, where T_0 is the characteristic time of the aging [14]. For the steady-state case, when aging and shear rejuvenation at a given shear rate $\dot{\gamma}_e$ cancel each other out, the structure ceases to evolve:

$$\frac{D\lambda}{Dt} = 0 \Rightarrow \lambda_e = \frac{1}{1+(\alpha_1/\alpha_0)\dot{\gamma}_e\, e^{\alpha_2\dot{\gamma}}} \tag{2}$$

where λ_e is the value of the coherency parameter at equilibrium. The viscosity approaches an equilibrium value $\eta_e(\dot{\gamma}_e)$.

Experiments verify that thixotropic suspensions are described well by the Herschel–Bulkley model with time-dependent properties [6]. This model is a combination of the Bingham plastic and the power-law models. The former accounts for the finite yield stress that must be exceeded for flow to occur, while the latter takes nonlinear shearing effects into account. The material parameters of the model are assumed to be functions of the coherency parameter λ and hence of time

$$\tau = \left[\frac{\tau_0(\lambda)}{\dot{\gamma}} + K(\lambda)\dot{\gamma}^{n(\lambda)-1}\right]\mathbf{D} \tag{3}$$

where τ is the viscous shear stress tensor, $K(\lambda)$ is the consistency index, $n(\lambda)$ is the power-law index, $\tau_0(\lambda)$ is the yield stress and $\dot{\gamma}$ is the second invariant of the rate of strain tensor $\mathbf{D} = \nabla\mathbf{u} + (\nabla\mathbf{u})^T$.

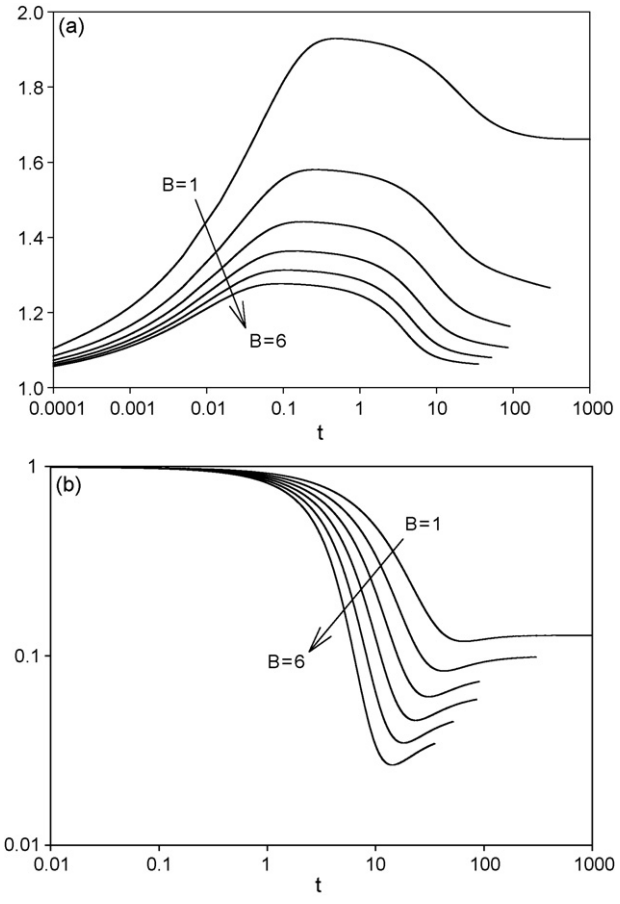

Fig. 9. Effects of the Bingham number B on (a) the length of the yielded domain and (b) the coherency parameter at the rotating surface; $a_0 = a_1 = a_2 = 0.01$ and $n = 0.5$.

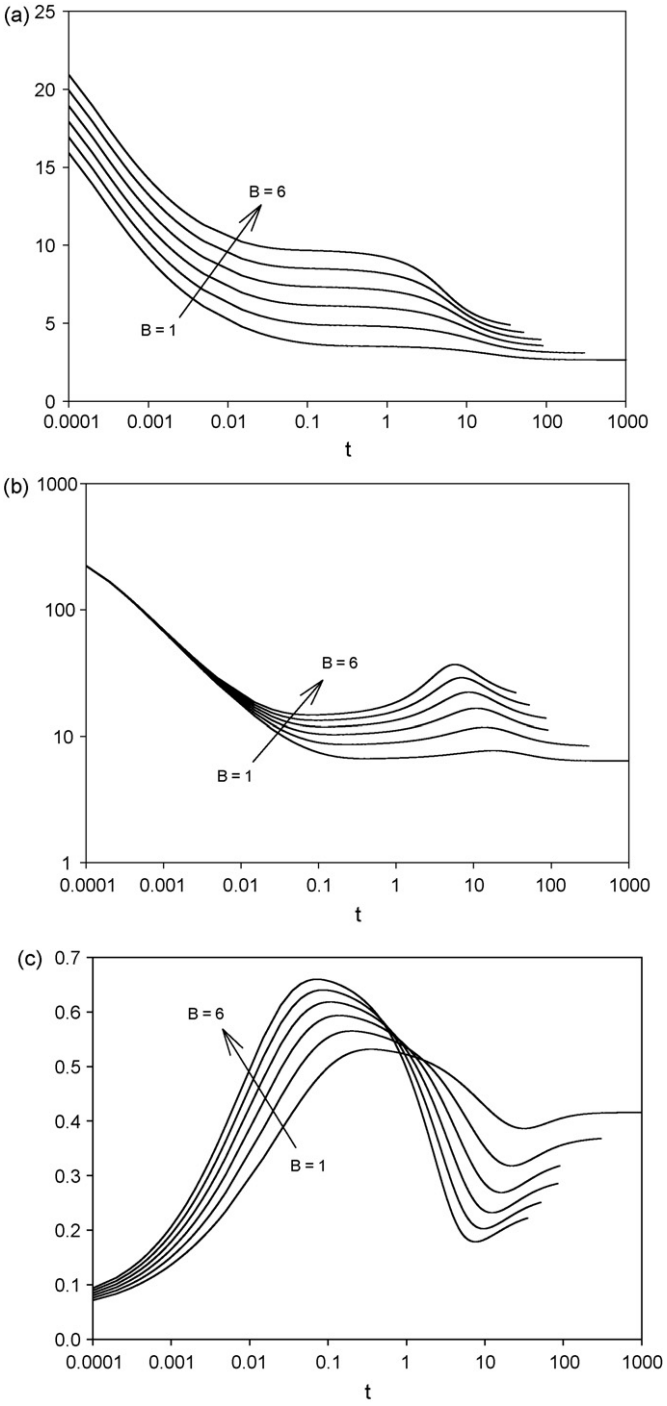

Fig. 10. Effects of the Bingham number B on (a) the shear stress, (b) the shear rate and (c) the viscosity at the rotating surface; $a_0 = a_1 = a_2 = 0.01$ and $n = 0.5$.

In a simple shear flow experiment Eq. (3) can be written in scalar form as follows

$$\tau = \tau_0(\lambda) + K(\lambda)\dot{\gamma}^{n(\lambda)} \tag{4}$$

The material parameters in the model, α_0, α_1 and α_2, and the equilibrium functions $K(\lambda)$, $n(\lambda)$ and $\tau_0(\lambda)$, can be estimated by stress versus time plots which are constructed using experimental steady-state data ($\dot{\gamma} = \dot{\gamma}_e$) [6]. For simplicity, it is assumed here that the equilibrium functions are constant, i.e. independent of the state of the structure.

The time-dependent function, $\tau_0(\lambda(t))$ must be defined a priori. In the present study a simple linear form

$$\tau_0(\lambda(t)) = \lambda(t)\tau_0 \tag{5}$$

is adopted. Of course, given sufficient information any other functional form can be readily used.

At steady-state $D\lambda/Dt = 0$ or when $\lambda = \lambda_e$ this model predicts flow curves of the type shown in Fig. 5. Despite the model's simplicity the predicted behavior is almost identical to recent experimental data for concentrated star polymer suspensions obtained by Beris et al. [23] and shown in Fig. 6. This provides a further verification of the validity of the theoretical model.

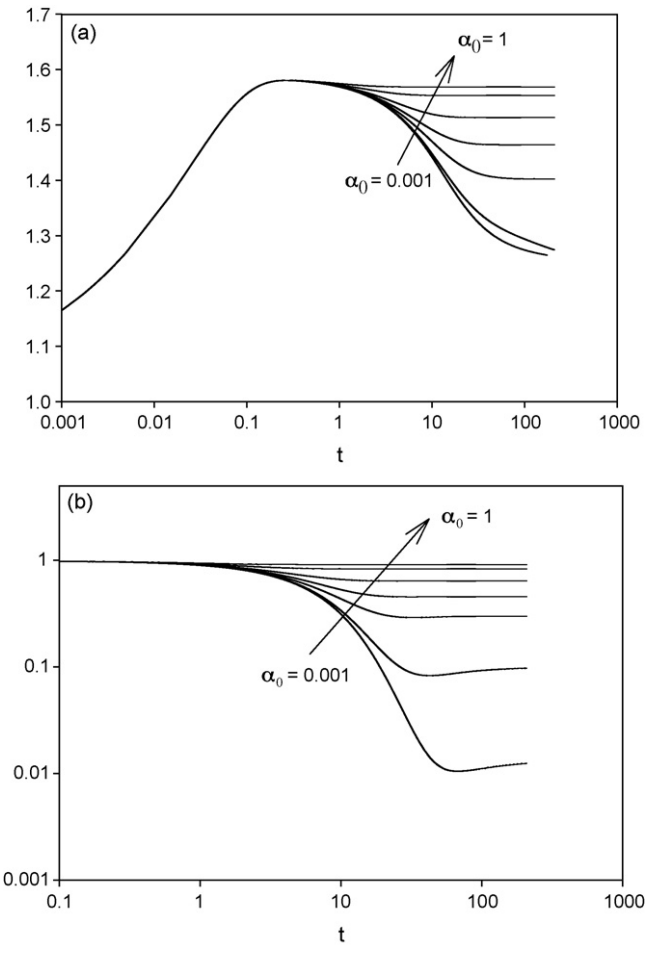

Fig. 11. . Effects of a_0 on (a) the length of the yielded domain and (b) the coherency parameter at the rotating surface; $B = 2$, $a_1 = a_2 = 0.01$, $n = 0.5$, $a_0 = 0.001$, 0.01, 0.05, 0.1, 0.2, 0.5, 1.0.

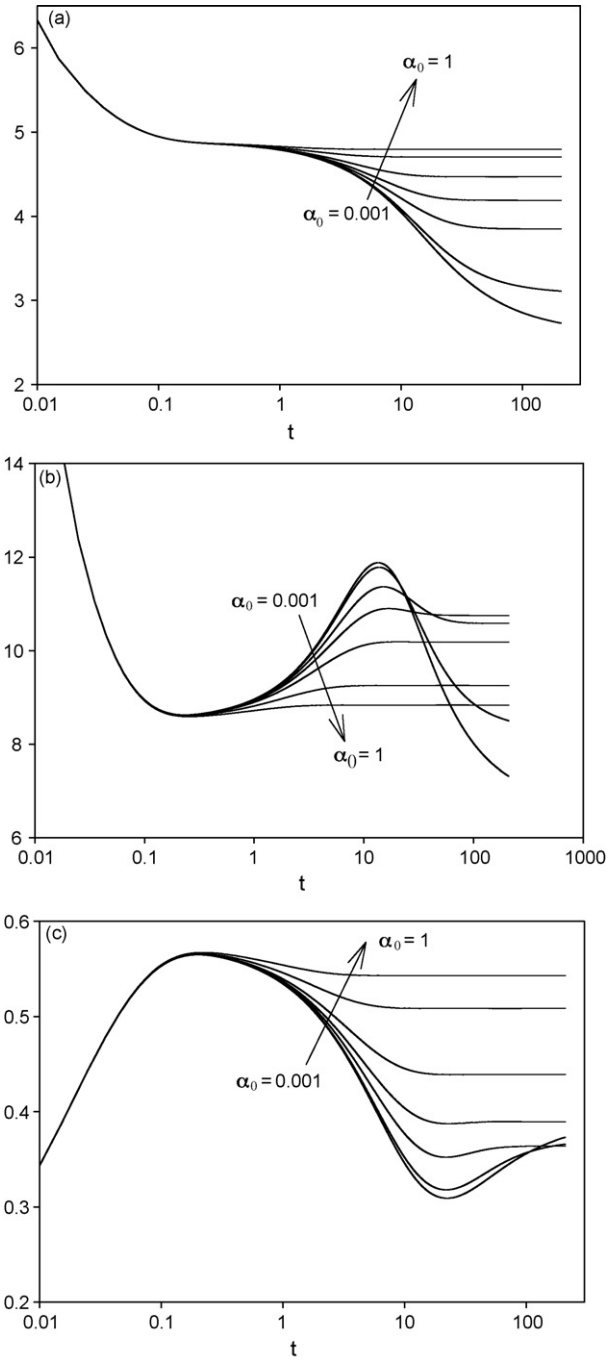

Fig. 12. Effects of a_0 on (a) the shear stress, (b) the shear rate and (c) the viscosity at the rotating surface; $B = 2$, $a_1 = a_2 = 0.01$, $n = 0.5$, $a_0 = 0.001$, 0.01, 0.05, 0.1, 0.2, 0.5, 1.0.

3. Flow in a rotational rheometer

We consider the flow of a thixotropic material in a classical rotational rheometer, schematically shown in Fig. 3. It is assumed that the globally imposed shear rate is constant and that shearing is isothermal, i.e. the temperature of the fluid remains constant throughout the experiment.

The conservation of linear momentum for the rotational flow of Fig. 3 is given by

$$\rho\frac{\partial u}{\partial t} = \frac{1}{r^2}\frac{\partial}{\partial r}(r^2\tau) \tag{6}$$

where u is the tangential velocity, $\tau = \tau_{r\theta}$, and ρ is the density. Eqs. (4) and (5) give

$$\tau = \lambda\tau_0 + K\dot{\gamma}^n \tag{7}$$

where

$$\dot{\gamma} = \left| r\frac{d}{dr}\left(\frac{u}{r}\right)\right|.$$

The angular velocity of the rotating shaft is ω, thus the tangential velocity of the fluid at the shaft is $u(R_1) = \omega R_1 = U$. In the unyielded region ($r_{max} \le r \le R_2$) the fluid is at rest.

For this simple shear flow experiment, Eq. (1) reduces to

$$\frac{\partial\lambda}{\partial t} = \alpha_0(1-\lambda) - \alpha_1\lambda\dot{\gamma}\, e^{\alpha_2\dot{\gamma}} \tag{8}$$

By using R_1, U, and $K(U/R_1)^{(n-1)}$ as scales respectively for length, velocity, and stress, the following dimensionless forms of Eqs. (6–8) are obtained:

$$Re\frac{\partial u'}{\partial t'} = \frac{1}{r'^2}\frac{\partial}{\partial r'}(r'^2\tau') \tag{9}$$

$$\tau' = \lambda B + \dot{\gamma'}^n \tag{10}$$

$$\frac{\partial\lambda}{\partial t'} = \alpha'_0(1-\lambda) - \alpha'_1\lambda\dot{\gamma'}\, e^{\alpha'_2\dot{\gamma'}} \tag{11}$$

where all the primed variables are dimensionless, and $Re = (\rho U R_1/K)(R_1/U)^{n-1}$ and $B = (\tau_0/K)(R_1/U)^n$ are, respectively, the generalized Reynolds and Bingham numbers. The primes will be dropped hereafter for simplicity.

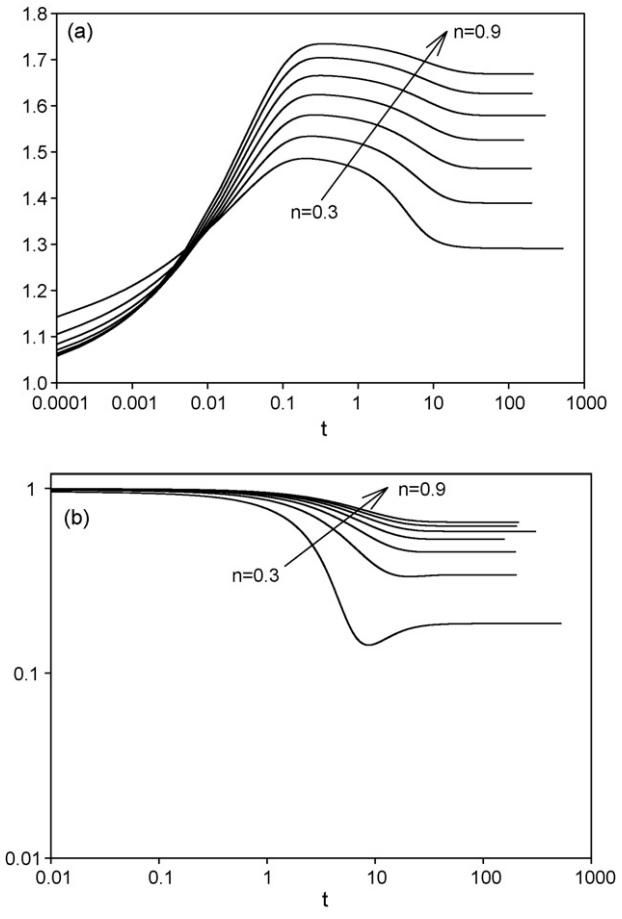

Fig. 13. Effects of n on (a) the length of the yielded domain and (b) the coherency parameter at the rotating surface; $B = 2$, $a_0 = 0.1$, $a_1 = a_2 = 0.01$.

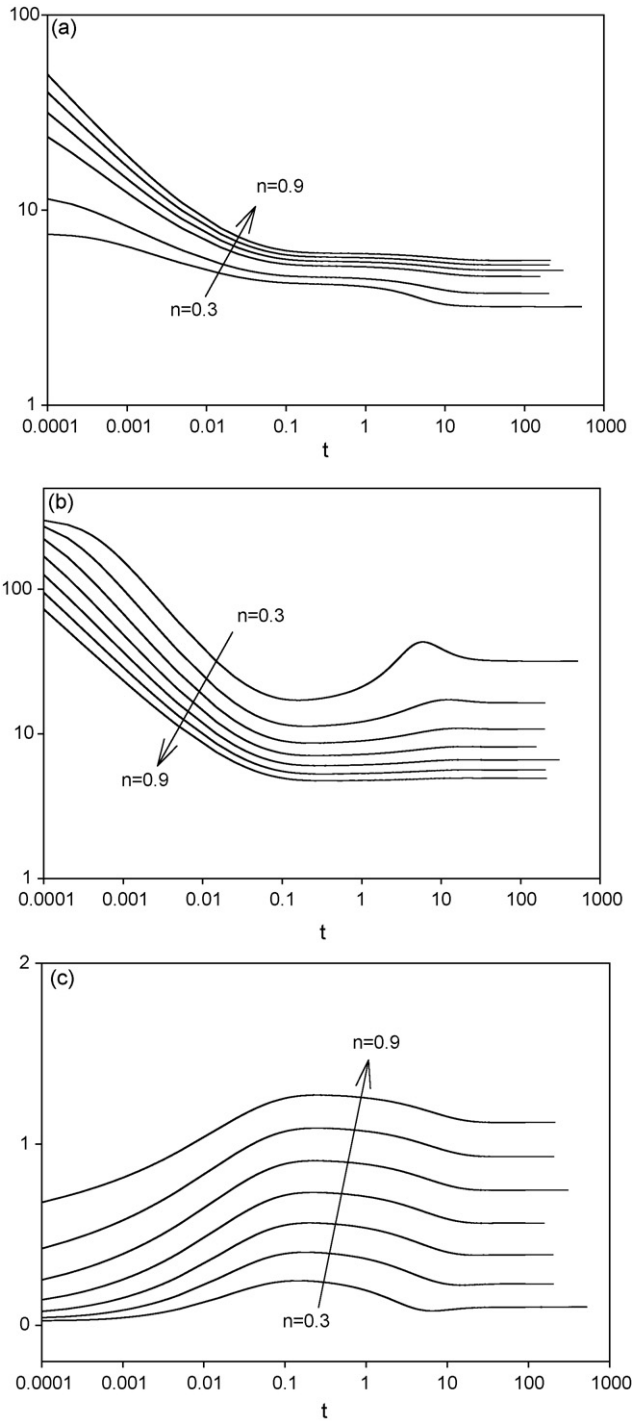

Fig. 14. Effects of n on (a) the shear stress, (b) the shear rate and (c) the viscosity at the rotating surface; $B = 2$, $a_0 = 0.1$, $a_1 = a_2 = 0.01$.

3.1. Method of solution

Since Herschel–Bulkley models are singular, obtaining an analytical solution is only possible for simple, steady and mostly unidirectional flows. In time-dependent and more geometrically complex flows the model should be regularized in order to remove the singularity and improve computational efficiency. A popular regularization is the one introduced by Papanastasiou which makes use of a smooth exponential function to represent the steep rise in the stress as the shear rate tends to zero [24].

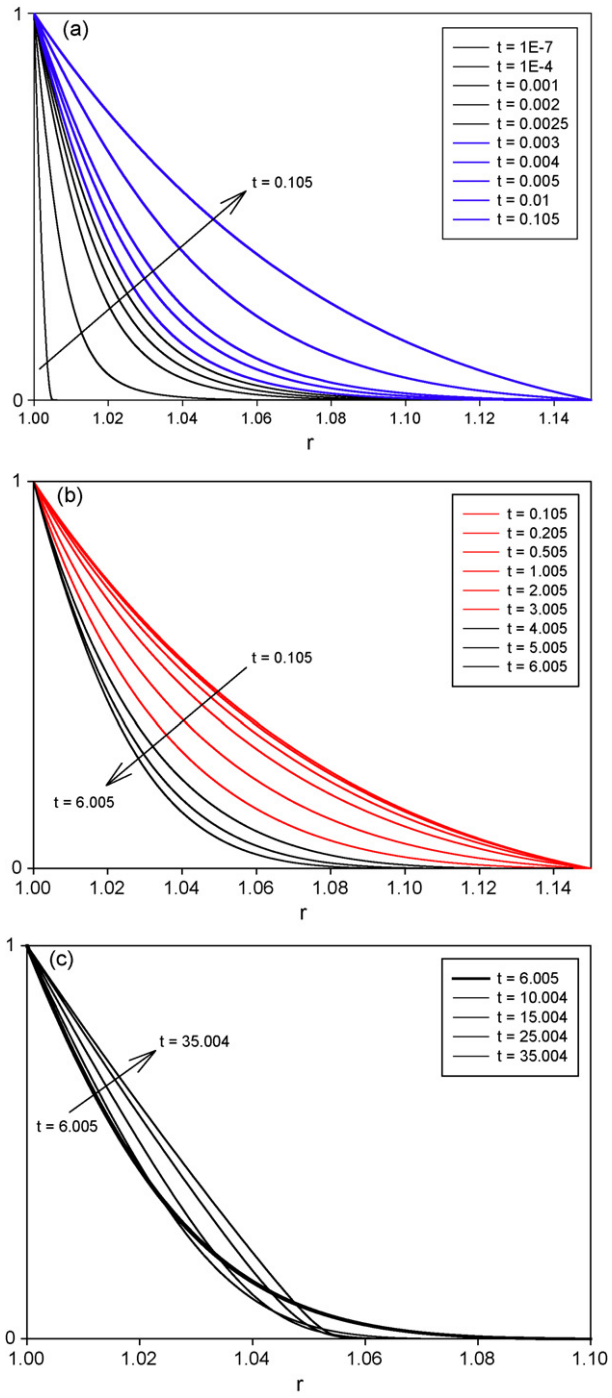

Fig. 15. Velocity distribution in the gap between the two concentric cylinders ($R_1 = 1$, $R_2 = 1.15$) as a function of time; $B = 6$, $a_0 = a_1 = a_2 = 0.01$ and $n = 0.5$.

The flow geometry of Fig. 3, allows the use of the inverse finite element method (IFEM) solution procedure [25]. In this method, the dependent variable (node velocity) is fixed and the solution is obtained for the independent variable (coordinates of the nodes) without inverting the equations. Here the velocity varies from 1 at the rotating end to 0 at the fixed surface. As shown in Fig. 4 the solution procedure determines the location of the nodes that correspond to a predefined velocity distribution. The advantages of this procedure, which is discussed in more detail in Ref. [1], are:

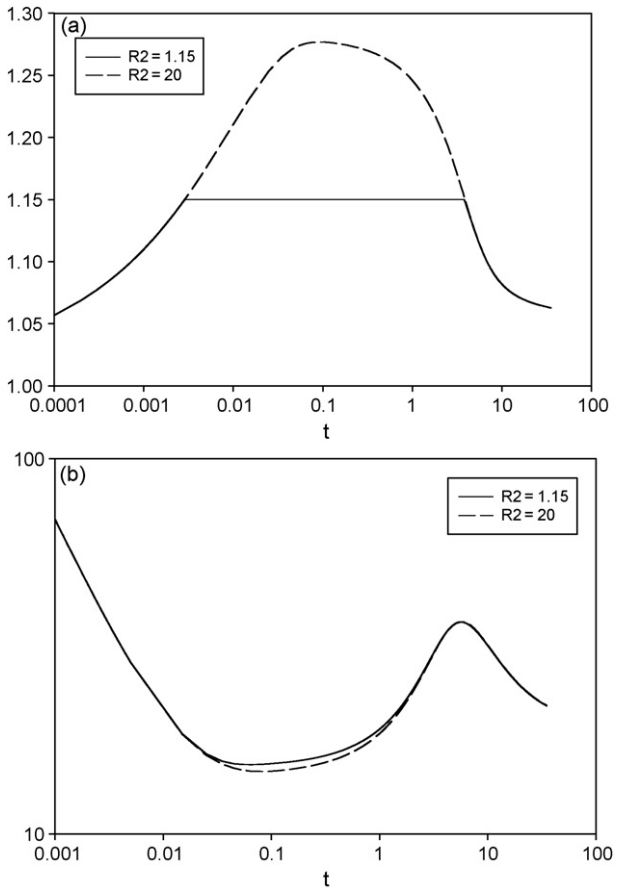

Fig. 16. The time evolutions of (a) the length of the yielded domain and (b) the shear rate at the rotating surface for $R_2 = 20$ and $R_2 = 1.15$; $B = 6$, $a_0 = a_1 = a_2 = 0.01$ and $n = 0.5$.

(a) Since the computational domain is limited to the yielded part of the fluid, the singularity no longer exists and the solution corresponds to the ideal constitutive model.
(b) The boundary conditions are applied and satisfied exactly.
(c) The method is ideal for studying stress shear banding not possible with standard computational methods.

The Jacobian of the Newton-Raphson procedure is saved using an element-by-element storage and solved by an iterative method

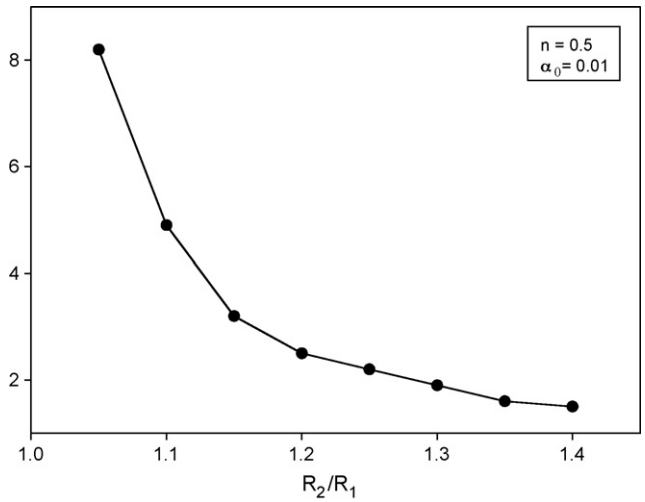

Fig. 17. The minimum B as a function of the outer radius for shear banding to occur.

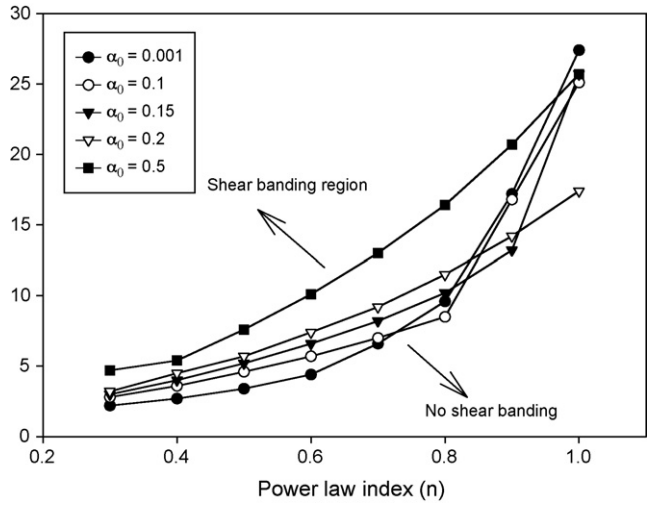

Fig. 18. The effect of B, n and a_0: shear banding occurs only for parameter combinations above the curves.

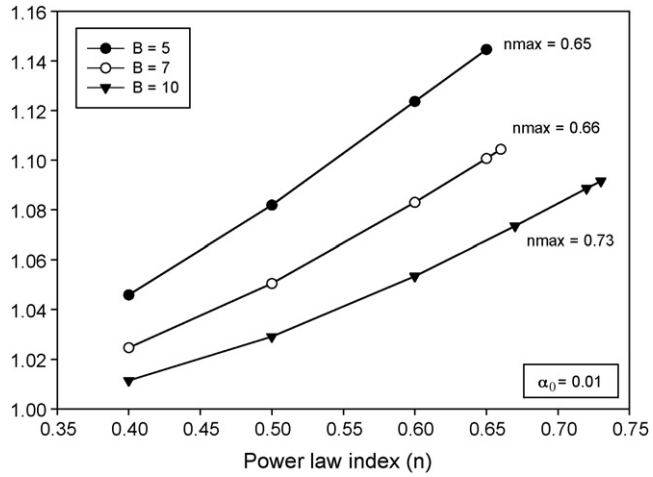

Fig. 19. The effect of B on the final shear band location for $a_0 = 0.01$.

based on a modification of the BiConjugate Gradient Stabilized Method [25,26]. The Jacobi preconditioning is used to speed up convergence. For converged results, usually two to three iterations in the Newton-Raphson procedure are necessary at each time step.

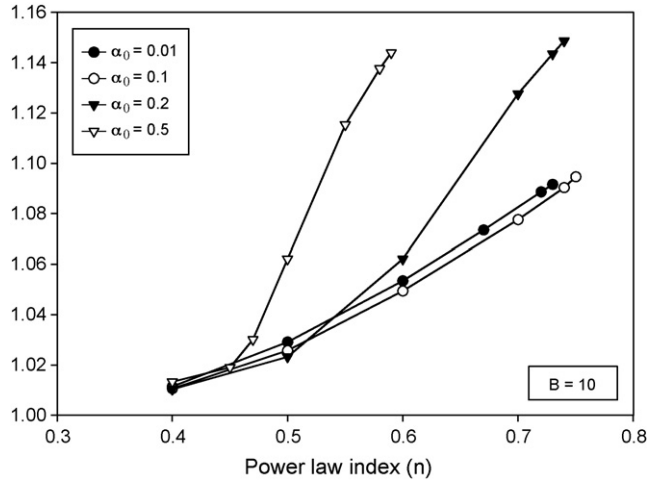

Fig. 20. The effect of a_0 on the final shear band location for $B = 10$.

The structure evolution equation (Eq. (11)) – corrected for the fact that the mesh moves with velocity u_m– is given by

$$\frac{d\lambda}{dt} = u_m \frac{\partial \lambda}{\partial r} + \alpha_0(1-\lambda) - \alpha_1 \lambda \dot{\gamma}\, e^{\alpha_2 \dot{\gamma}} \tag{12}$$

This is solved explicitly at each Newton-Raphson iteration step for each node using high-order finite difference approximation for the velocity gradient subject to the proper boundary conditions:

(a) At the early stages of shearing $r = r_{max}$ and $\lambda = 1.0$. In this case r_{max} is unknown and it is determined by the solution procedure.
(b) When the material within the gap yields completely the last node is fixed at the location of the second cylinder i.e. $r = R_2$ and it is treated as known. The parameter λ is evaluated using Eq. (12).
(c) In cases where the yielded front retreats the location of the last node is treated as unknown as in case (a) and λ is evaluated again using Eq. (12).

4. Results and discussion

Since Re is a multiplying factor in Eq. (9) we obtain results only for Re = 1. Changing its value leads only to a different time scale. All simulations start with an arbitrary small yielded domain ($1 \le r < 1 + \varepsilon$). Numerically this one-dimensional problem is quite stiff and care must be exercised in the selection of the mesh and time discretizations. For mesh-independent results a total of 40 one-dimensional quadratic elements is used and ε is set to 0.005. The time step used for stable solutions is of the order of 10^{-7}; however, the step is adjusted internally by the code (up to 10^{-2}) during the simulation.

4.1. Aging and shear rejuvenation in partially yielded material

Fig. 7 shows the evolution of the shear rate, the shear stress, the coherency parameter and the viscosity ($n = \tau/\dot{\gamma}$) at the rotating surface, as well as the evolution of the length of the yielded domain, in a typical flow with $B = 2$, $a_0 = a_1 = a_2 = 0.01$ and $n = 0.5$. In this and all subsequent simulations of partially yielded material, the radius R_2 of the outer cylinder is larger than the maximum length of the yielded domain (r_{max}). The default value of R_2 is set to a large value of 20. Of course this is an unnecessarily large value since in all cases examined the yielded domain never exceeds the value of 2.

Upon shearing the length of the yielded domain increases rapidly to a quasi-steady-state which is independent of ε and then drops to a final steady value. The shear stress at the rotating cylinder undergoes a typical sigmoidal variation as shown in experiments [12]. Again this is a further demonstration of the validity of the model. On the other hand, the shear rate drops from an initially large value gradually to a minimum value. As soon as the yielded domain starts retreating (after its quasi-steady-state) the shear rate rises again as a result of the fluid being confined to a smaller region. The shear rate reaches a maximum and then drops approaching a steady-state value. Shortly after the shear rate starts decreasing the coherency parameter reaches a minimum and the buildup term in Eq. (11) relatively increases. Therefore, the coherency parameter reaches a minimum (breakdown and buildup cancel each other out) and then increases (aging of the fluid structure) before reaching a steady-state, where the buildup and breakdown terms are equal. Upon the application of shear, the viscosity increases quite fast and reaches a maximum. As soon as the shear rate starts increasing the viscosity decreases and reaches a minimum when the shear rate reaches a maximum. As the shear rate starts to fall for the second time the viscosity increases and reaches a steady-state value. This complex behavior necessitates the need for more sophisticated tools for the determination of unsteady material constants.

Fig. 8 shows the steady-state or equilibrium distribution of the coherency parameter, the shear rate, the shear stress and the viscosity, along the radial direction in the yielded region. The coherency parameter increases gradually with r from a very low value at the rotating cylinder surface; however, at some point very close to the yield point a steep increase occurs. The coherency parameter tends asympotically to unity at the yield point, which indicates a fully connected internal structure. The shear stress decreases almost linearly along the length of the yielded region. The shear rate starts from a finite value at the rotating surface and drops to zero at the yield point. At the region where there is a steep increase in the coherency parameter the rate at which the shear rate decreases is much faster. The viscosity increases almost linearly with the radial distance. However, at the region where the rate of decrease of the shear rate is very large the viscosity increases sharply and becomes practically infinite at the yield point.

Figs. 9 and 10 show the effects of the Bingham number B on the length of the yielded domain, and the coherency parameter, the shear stress, the shear rate and the viscosity at the rotating surface, respectively for $a_0 = a_1 = a_2 = 0.01$ and $n = 0.5$. While the coherency parameter and the length of the yielded domain decrease with B, the shear stress and shear rate at the rotating surface increase. This is expected as the strength of the suspension increases with the yield stress and hence with B. As a result of the shear stress and shear rate variations, the viscosity increases with B immediately upon shearing and decreases with B for times larger than ~0.5 to ~1.6 s (depending on B).

The effect of the recovery coefficient on all quantities of interest is illustrated in Figs. 11 and 12, where results for $B = 2$, $a_1 = a_2 = 0.01$ and $n = 0.5$ are shown. The quasi-steady-state value of the length of the yielded domain is unaffected by a_0 (Fig. 11a); however, its value clearly increases with a_0 as the flow develops further. The reason is that for large values of a_0 the strength of the fluid is sufficient to support shearing over a larger yielded region. As expected, the coherency parameter increases with a_0 (Fig. 11b). During the early stages of shearing the shear stress does not vary with a_0; this increases with a_0 about one second after flow is initiated. This is expected as the strength of the suspension during shearing does not decrease as much for larger recovery coefficients. This behavior supports the assumption that buildup can be negligible for short-term transients [1].

For large values of a_0 the variation of the shear stress is exponential and not sigmoidal. As expected the shear rate decreases with a_0. Even though the maximum of the shear rate curve decreases with a_0 the shear rate after this maximum drops faster for very small coefficients but its steady-state value is smaller. The viscosity increases with a_0 but its steady-state value follows a non-monotonic variation at very small a_0. Generally, the larger the coefficient the sooner the system reaches an equilibrium state.

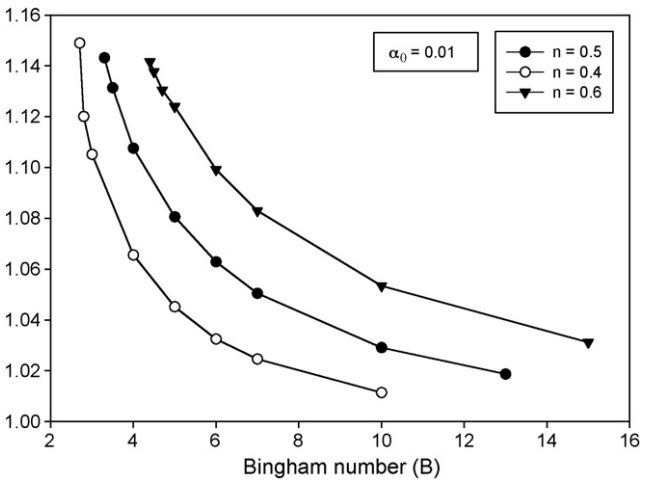

Fig. 21. The effect of n on the final shear band location for $a_0 = 0.01$.

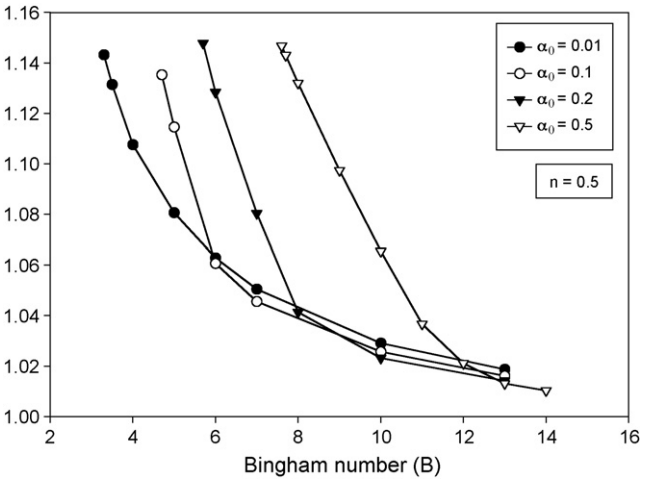

Fig. 22. The effect of a_0 on the final shear band location for $n = 0.5$.

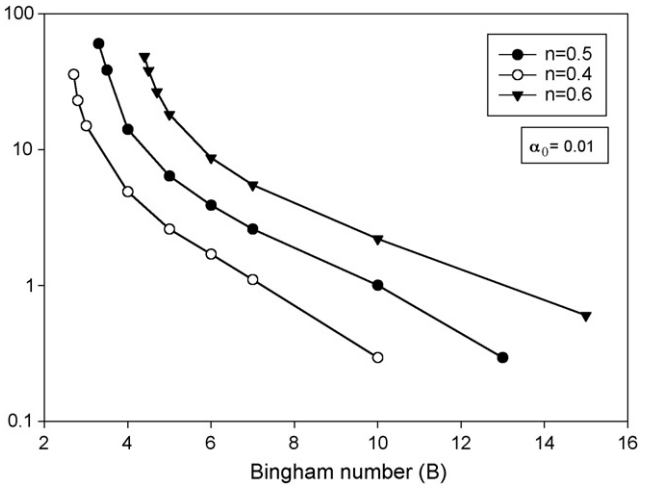

Fig. 23. Retreat time as a function of the Bingham number for various values of n and $a_0 = 0.01$.

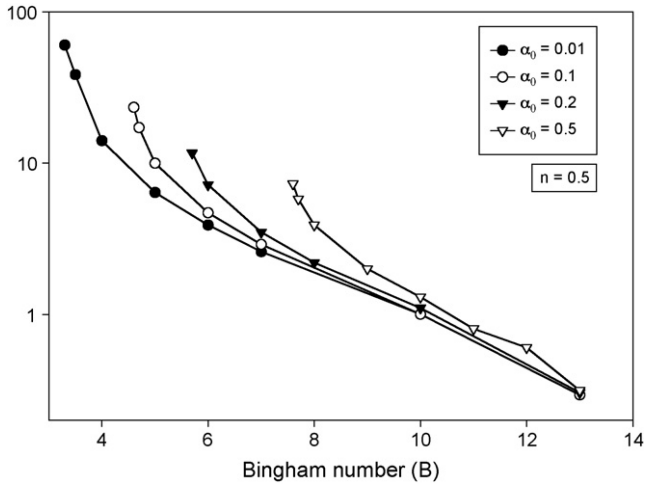

Fig. 24. Retreat time as a function of the Bingham number for various values of a_0 and $n = 0.5$.

Table 1
Final shear band location for various parameter combinations.

	n	B					
		2	3	4	5	6	7
a_0							
0.001	0.4	–	1.1091	1.0683	1.0465	1.0333	1.0247
	0.5	–	–	1.1121	1.0832	1.0645	1.0515
	0.6	–	–	–	1.1250	1.1015	1.0846
	0.7	–	–	–	–	–	1.1261
0.005	0.4	–	1.1067	1.0669	1.0459	1.0329	1.0244
	0.5	–	–	1.1097	1.0819	1.0638	1.0510
	0.6	–	–	–	1.1237	1.1003	1.0849
	0.7	–	–	–	–	–	–
0.01	0.4	–	1.1052	1.0656	1.0452	1.0325	1.0246
	0.5	–	–	1.1076	1.0806	1.0629	1.0505
	0.6	–	–	–	1.1240	1.0992	1.0830
	0.7	–	–	–	–	–	–
0.05	0.4	–	–	1.0663	1.0430	1.0297	1.0232
	0.5	–	–	1.1209	1.0751	1.0586	1.0473
	0.6	–	–	–	1.1256	1.0935	1.0783
	0.7	–	–	–	–	–	–
0.1	0.4	–	–	1.1027	1.0463	1.0299	1.0220
	0.5	–	–	–	1.1146	1.0607	1.0456
	0.6	–	–	–	–	1.1310	1.0856
	0.7	–	–	–	–	–	–
0.2	0.4	–	–	–	1.0881	1.0370	1.0236
	0.5	–	–	–	–	1.1284	1.0804
	0.6	–	–	–	–	–	–
	0.7	–	–	–	–	–	–
0.5	0.4	–	–	–	–	1.1127	1.0589
	0.5	–	–	–	–	–	–
	0.6	–	–	–	–	–	–
	0.7	–	–	–	–	–	–
1.0	0.4	–	–	–	–	–	–
	0.5	–	–	–	–	–	–
	0.6	–	–	–	–	–	–
	0.7	–	–	–	–	–	–

Figs. 13 and 14 show the effect of the power-law index n. The length of the yielded domain increases with n, except during the very early stages of the flow initiation. Unlike the shear rate, the coherency parameter, shear stress and viscosity at the rotating cylinder increase with n. It is interesting to note that the time for reaching equilibrium is practically independent of n.

4.2. Shear banding

To illustrate the shear banding phenomenon R_2 is set to 1.15. It is important to repeat here that, except for a simple unsnapping rule described below for the node fixed to the outer boundary at the instant the yielded domain starts to retreat, these results are obtained automatically without user intervention due to the novelty of the solution procedure: the method tracks at all times the yielded domain free of any mathematical singularities by satisfying exactly all boundary conditions, governing equations and constitutive relations without regularization.

Fig. 15 shows the evolution of the velocity distribution between the two concentric cylinders when $B=6$, $a_0=a_1=a_2=0.01$ and $n=0.5$. The velocity varies from unity at R_1 to zero at R_2. As soon as the yielded material reaches the fixed cylinder, the velocity increases throughout the entire gap (Fig. 15a). As the shearing continues the material breaks down, the velocity decreases everywhere within the gap and shear banding occurs (Fig. 15b). When the yielded material retreats sufficiently, the velocity in the yielded region increases and reaches equilibrium when the shear band location attains a steady value (Fig. 15c). At equilibrium the velocity except close to the fixed cylinder varies almost linearly within the yielded region.

Computationally retreating is first signaled when the nodal velocities ($u_m = dr_i/dt$) of the nodes adjacent to the node fixed to the outer cylinder assume negative values and the aspect ratio of the associated elements start to differ by a set percentage. Then, when the shear rate at the node decreases to a small value close to zero the rule is activated when the next change in the shear goes through a sign reversal: the fixed node is reclassified as a "free" node and its current location is set to a value slightly smaller than R_2 to $R_2 - 1.0\text{E}^{-6}$. Its new location is calculated according to the solution procedure. If the calculated location is less than R_2 no other action is taken, otherwise its value is set again to $R_2 - 1.0\text{E}^{-6}$. The time integration is continued normally by maintaining the classification of the node as "free". Actually the rule is optimized for most simulations performed to ensure that once implemented the above adjustment is not repeated for more than a couple of time steps. Therefore, given the normally small time integration steps used in these simulations and that each simulation typically takes several million time steps to complete, this simple rule produces smooth solutions without irregularities that can be documented. In all simulations performed, at the instant of retreating there was no tendency for physical oscillations of the yielded domain.

As shown in Fig. 16a the yielded domain for a fixed cylinder at $R_2=1.15$ retreats following the exact same "path" as the yielded domain in the case of partially yielded material (where the default value is set at $R_2=20$). Here the fixed cylinder is placed

Table 2
Retreat time for various parameter combinations.

a_0	n	B					
		2	3	4	5	6	7
0.001	0.4	–	13.4	4.8	2.6	1.7	1.1
	0.5	–	–	13.0	6.2	3.8	2.6
	0.6	–	–	–	16.6	8.4	5.4
	0.7	–	–	–	–	–	25.4
0.005	0.4	–	14.0	4.8	2.6	1.7	1.1
	0.5	–	–	13.5	6.3	3.8	2.6
	0.6	–	–	–	17.3	8.5	5.5
	0.7	–	–	–	–	–	–
0.01	0.4	–	15.0	4.9	2.6	1.7	1.1
	0.5	–	–	14.1	6.4	3.9	2.6
	0.6	–	–	–	18.2	8.7	5.5
	0.7	–	–	–	–	–	–
0.05	0.4	–	–	5.5	2.8	1.7	1.1
	0.5	–	–	26.1	7.5	4.2	2.7
	0.6	–	–	–	32.8	11.0	6.3
	0.7	–	–	–	–	–	–
0.1	0.4	–	–	6.9	3.0	1.8	1.2
	0.5	–	–	–	10.4	4.7	2.9
	0.6	–	–	–	–	19.0	7.7
	0.7	–	–	–	–	–	–
0.2	0.4	–	–	–	3.6	1.9	1.2
	0.5	–	–	–	–	7.2	3.5
	0.6	–	–	–	–	–	–
	0.7	–	–	–	–	–	–
0.5	0.4	–	–	–	–	2.8	1.5
	0.5	–	–	–	–	–	–
	0.6	–	–	–	–	–	–
	0.7	–	–	–	–	–	–
1.0	0.4	–	–	–	–	–	–
	0.5	–	–	–	–	–	–
	0.6	–	–	–	–	–	–
	0.7	–	–	–	–	–	–

between the quasi-steady-steady and the steady-state value of the length of the yielded region. Therefore, the fixed cylinder position is critical and it determines whether shear banding occurs or not. When the material in the gap between the two cylinders is fully yielded (i.e. the extent of the yielded domain reaches the fixed boundary at $R_2 = 1.15$) the local shear rate increases to compensate for the confinement of the fluid by the fixed cylinder (Fig. 16b). Importantly, Fig. 17 shows the minimum value of B required for banding to occur as a function of the outer radius R_2.

Fig. 18 shows the effect of B, n and a_0 on shear banding. The latter occurs only for parameter combinations above the curves. For combinations below the curves the material between the two cylinders is completely yielded. It is clearly shown that for values of n up to about 0.7 the minimum Bingham number (B) for which shear banding occurs increases with a_0. For larger values of n the stress and shear rate in the material are quite large (i.e. the material brakes down more easily). Therefore, only large (>0.2) values of a_0 can significantly affect the flow. As a result, for small a_0 a large B is required to cause shear banding. The opposite happens for larger values of a_0.

Fig. 19 shows the effect of B on the final shear band location for various n and $a_0 = 0.01$. As B increases the final shear band location decreases and the maximum n – for which shear banding occurs – increases. Fig. 20 shows the effect of a_0 on the final shear band location for various n and $B = 10$. For small n the final shear band location is practically unaffected by a_0; it decreases only slightly with a_0 (0.01–0.2). The same occurs for small a_0 (0.01 and 0.1). For larger a_0 (0.2 and 0.5) shear banding occurs at lower n and the final location of the band increases.

Fig. 21 shows the effect of n on the final shear band location as a function of B and $a_0 = 0.01$. The final shear band location increases with n. Values of B that result in fully unyielded material are not included in the results. Fig. 22 shows the effect of a_0 on the final shear band location as a function of B and $n = 0.5$. The final shear band location increases with a_0. For larger values of B, however, the effect of a_0 is not significant; the final shear band location decreases only slightly with a_0.

Fig. 23 shows the effect of n on the retreat time for various B and $a_0 = 0.01$. The retreat time, defined as the time during which the material within the gap remains fully yielded, clearly increases with n. This is because when the yielded material reaches the fixed cylinder and the stress and shear rate at that point start to increase, they reach a larger maximum value as n increases. Therefore, more time is needed for these two quantities to drop to zero in order for the yielded domain to start retreating. Fig. 24 shows the effect of a_0 on the retreat time as a function of B and $n = 0.5$. The retreat time increases with a_0 even though the effect is not as pronounced for large values of B.

Results for the final shear band location and retreat time are shown in Tables 1 and 2 respectively, for various parameters. It is clearly shown that the final shear band location and retreat time variables increase with a_0 and n and decrease with B. However, for small values of a_0 (≤ 0.01), the final shear band location is practically unaffected, whereas retreat times increase slightly with a_0. As the Bingham number increases the effect of a_0 is less pronounced.

5. Conclusions

The flow of a yield stress material (e.g. semisolid suspension) in a concentric cylindrical rheometer has been simulated. The short and long-term responses of the material have been modeled using the Herschel–Bulkley fluid model and the effects of shear rejuvenation, aging and shear banding have been investigated.

Shear rejuvenation and aging have been studied in partially yielded material by setting the radius of the fixed outer cylinder at a large default value ($R_2 = 20$, $R_1 = 1$). Upon shearing, the material breaks down resulting in the decrease of the stress and shear rate at the rotating surface and along the length of the yielded domain. The latter initially increases reaching a quasi-steady-state value and then drops to an equilibrium value. Therefore, two regions are created: the yielded and the unyielded one. At early stages, shear rejuvenation dominates the evolution of the structure. After a very long time, the rates of breakdown and buildup become equal canceling each other and the material attains an equilibrium state (all the variables acquired steady-state-values). At the maximum length of the yielded region (yield point) the shear rate is zero and the viscosity is infinite, at all times.

Shear banding has been investigated by setting the radius of the fixed cylinder at $R_2 = 1.15$. It has been shown that in addition to the physical parameters shear banding also depends on the flow geometry. Even for large values of the outer radius the yielded region eventually retreats provided the local shear rate and the structural parameter at the outer cylinder (Figs. 9a, 11a and 13a) are sufficiently low. When R_2 is set below the steady-state length of the yielded region shear banding is not observed. Various experiments reported in the literature have shown that shear banding occurs below a critical globally imposed shear rate [13]. This is true provided the position of the fixed cylinder is set between the maximum and the steady-state values of the length of the yielded region (Fig. 16a). Fluids with large buildup coefficients reach equilibrium in relatively short time which may be important in shearing applications. Additionally, the buildup coefficient must be at least an order of magnitude larger than the breakdown coefficient in order to significantly affect the flow.

Shear rejuvenation, aging and shear banding are important phenomena in thixotropic shear thinning of yield stress fluids. The effects of the various fluid parameters and flow geometry on those phenomena must be known in order to accurately predict the fluid behavior under various shearing conditions. Computational rheology provides a meaningful, fast and certainly cost-effective means to determine material constants from rheological tests provided of course it is accompanied by appropriate models and underlying assumptions.

Finally as a cautionary note, we should admit that modeling thixotropic effects has some inherent difficulties. The structural parameters used are not necessarily directly measurable and different models of structure evolution may be well able to reproduce a given data set. The approach is thus necessarily phenomenological. Similar critiques may be leveled at other branches of mechanics and thermodynamics, which are awash with 'internal variables'. Such critiques do not invalidate the study of the phenomena and should not prevent the advancement of knowledge, by postulating appropriate models that fit reasonably with the available data, as we have done here. Ideally of course we would like to be able to directly validate any given structure evolution model. It is hard to envisage experiments that can do this, and in the case of semisolid metals there are additional constraints.

Acknowledgement

One of the authors (GG) was partially supported by the Greek General Secretariat for Research and Technology (Basic Research Program PENED, -03ED566).

References

[1] A.N. Alexandrou, G. Georgiou, On the early breakdown of semisolid suspensions, J. Non-Newtonian Fluid Mech. 142 (2007) 199–206.
[2] G.D. Parfitt (Ed.), Dispersion of Powders in Liquids, Applied Science, New Jersey, 1981.
[3] V.C. Kelessidis, R. Maglione, Modeling rheological behavior of bentonite suspensions as Casson and Robertson-Stiff fluids using Newtonian and true shear rates in Couette viscometry, Powder Technol. 168 (2006) 134–147.
[4] P. Coussot, F. Bertrand, B. Herzhaft, Rheological behavior of drilling muds: characterization using MRI visualization, Oil Gas Sci. Technol.: Rev. IFP 59 (2004) 23–29.
[5] B. Paiuk, D. Oakley, C. Rodriguez, L.E. Capuano Jr., The influence of bentonite source on the use of mixed metal oxide drilling fluid systems for geothermal drilling, Geotherm. Resour. Council Trans. 28 (2004) 163–168.
[6] G.R. Burgos, A.N. Alexandrou, V.M. Entov, Thixotropic behavior of semisolid slurries, J. Mater. Process. Technol. 110 (2001) 164–176.
[7] H.A. Barnes, J.F. Hutton, K. Walters, An Introduction to Rheology, Elsevier Science, Amsterdam, 1989.
[8] G. Harrison, G.V. Franks, V. Tirtaatmadja, D.V. Boger, Suspensions and polymers—common links in rheology, Korea-Aust. Rheol. J. 11 (1999) 197–218.
[9] H.A. Barnes, Thixotropy—a review, J. Non-Newtonian Fluid Mech. 70 (1997) 1–33.
[10] J. Mewis, Thixotropy—a general review, J. Non-Newtonian Fluid Mech. 6 (1979) 1–20.
[11] J. Ferguson, Z. Kemblowski, Applied Fluid Rheology, Elsevier Applied Science, Cambridge, 1991.
[12] N. Tonmukayakul, Q.Y. Pan, A.N. Alexandrou, D. Apelian, Transient flow characteristics and properties of semi-solid aluminum alloy A356, in: 8th International Conference on Semi-Solid Processing of Metals and Alloys, September 21–23, Limassol, Cyprus, 2004.
[13] W.B. Russel, D.A. Saville, W.R. Schowalter, Colloidal Dispersions, Cambridge University Press, Cambridge, 1989.
[14] P. Coussot, Q.D. Nguyen, H.T. Huynh, D. Bonn, Viscosity bifurcation in thixotropic, yielding fluids, J. Rheol. 46 (2002) 573–589.
[15] P.C.F. Moller, J. Mewis, D. Bonn, Yield stress and thixotropy: on the difficulty of measuring yield stresses in practice, Soft Matter 2 (2006) 274–283.
[16] F. Pignon, A. Magnin, J.-M. Piau, Thixotropic behavior of clay dispersions: combinations of scattering and rheometric effects, J. Rheol. 42 (1998) 1349–1373.
[17] B. Abou, D. Bonn, J. Meunier, Aging dynamics in a colloidal glass, Phys. Rev. E 64 (2001) 021510.
[18] N. Huang, G. Ovarlez, F. Bertrand, S. Rodts, P. Coussot, D. Bonn, Flow of wet granular materials, Phys. Rev. Lett. 94 (2005) 028301.
[19] P. Coussot, J.S. Raynaud, F. Bertrand, P. Moucheront, J.P. Guilbaud, H.T. Huynh, S. Jarny, D. Lesueur, Coexistence of liquid and solid phases in flowing soft-glassy materials, Phys. Rev. Lett. 88 (2002) 218301.
[20] V. Bertola, F. Bertrand, H. Tabuteau, D. Bonn, P. Coussot, Wall slip and yielding in pasty materials, J. Rheol. 47 (2003) 1211–1226.
[21] M. Mada, F. Ajersch, Thixotropic effects in semi-solid Al – 6%Si alloy reinforced with SiC particles, in: R.B. Bhagat, et al. (Eds.), Metal & Ceramic Matrix Composites: Processing Modeling & Mechanical Behavior, The Minerals, Metals and Materials Society, 1990, pp. 337–350.
[22] H. Peng, K.K. Wang, Steady-state and transient rheological behavior of a semisolid tin-lead alloy in simple shear flow, in: D.H. Kirkwood, P. Kapranos (Eds.), 4th International Conference on Semi-Solid Processing of Alloys and Composites, The University of Sheffield, England, 1996, pp. 2–9.
[23] A.N. Beris, E. Stiakakis, D. Vlassopoulos, A thermodynamically consistent model for the thixotropic behavior of concentrated star polymer suspensions, J. Non-Newtonian Fluid Mech. 152 (2008) 76–85.
[24] T.C. Papanastasiou, Flows of materials with yield, J. Rheol. 31 (1987) 385–404.
[25] A.N. Alexandrou, An inverse finite element method for directly formulated free boundary problems, Int. J. Numer. Methods Eng. 28 (1989) 2383–2396.
[26] H. Van Der Vorst, Bi-CGSTAB: a fast and smoothly converging variant of Bi-CG for the solution of nonsymmetric linear systems, SIAM J. Sci. Stat. Comput. 13 (1992) 631–644.